Materials Today Advances 8 (2020) 100084

Contents lists available at ScienceDirect

Materials Today Advances

journal homepage: www.journals.elsevier.com/materials-today-advances/

Microcomputed tomography–based characterization of advanced materials: a review

L. Vásárhelyi [a], Z. Kónya [a, b], Á. Kukovecz [a], R. Vajtai [a, c, *]

[a] Interdisciplinary Excellence Centre, Department of Applied and Environmental Chemistry, University of Szeged, H-6720, Rerrich Béla Tér 1, Szeged, Hungary
[b] MTA-SZTE Reaction Kinetics and Surface Chemistry Research Group, H-6720 Szeged, Rerrich sq. 1, Hungary
[c] Department of Materials Science and NanoEngineering, Rice University, 6100 Main Street, Houston, TX 77005, USA

ARTICLE INFO

Article history:
Received 15 April 2020
Received in revised form
11 May 2020
Accepted 11 May 2020
Available online xxx

Keywords:
Micro-CT
X-ray
Bioinspired materials
Energy and environment
Structural materials
Porous rock
Energy storage
Filtration

ABSTRACT

Micro-computed tomography (CT) is an X-ray tomography technique with (sub)micron resolution, typically using an X-ray tube with cone-beam geometry as a source and a rotating sample holder. While conventional CT maintained a strong position in life science and low-resolution high-energy CT became widespread in industrial quality control, micro-CT has enjoyed a boost in interest from the materials science research community in the past decade. The key reasons behind this are the versatile, non-destructive nature of micro-CT as a characterization method offering also in situ and in operando possibilities and the fact that micro-CT has become indispensable in developing and verifying computational material models as well. The goal of the present mini review is to give a concise introduction of the method to newcomers and showcase a few impressive recent results that can help in devising even more innovative future uses of micro-CT. After a brief overview of alternative three-dimensional imaging techniques, we review the basics of micro-CT covering important concepts such as resolution, magnification, and the Hounsfield unit. The second part of the article summarizes characteristic materials science micro-CT applications in bioinspired materials, structural materials, porous natural materials, energy storage, energy conversion, and filtration.

1. Introduction

The microstructure of materials largely determines their mechanical and physical attributes and behavior. Therefore, imaging the inner structure and morphological characteristics of materials is of paramount importance in material design and engineering. The inherent limitation of two-dimensional (2D) imaging methods is their inability to provide spatial information about the investigated structure. On the other hand, three-dimensional (3D) imaging can reveal the volume, shape, spatial and size distribution, and connectivity of inhomogeneities (e.g. pores, different phases, cracks). For example, 2D radiographs can confirm the existence of cracks, discontinuities, pores, or structural errors, but 3D images can also help us localize them and identify their origin.

1.1. 3D imaging techniques

Most 3D imaging techniques work with electromagnetic waves (the exception being ultrasonic tomography), and the wavelength of the applied radiation determines the scale of the features investigated. The theoretical resolution limit when using visible light is approximately 200 nm, while with electrons even individual atoms can be investigated.

The entry point into the world of 3D imaging is confocal optical microscopy that allows examining the 3D structure in a finite deepness and for transparent materials only. (Although opaque samples can also be studied in fluorescence mode.)

Magnetic resonance imaging provides fully resolved 3D images non-invasively and non-destructively using the resonance signal of hydrogen atoms. Excellent for soft tissues (it is the highest contrast medical imaging technique), its highest resolution is a couple of tens of micrometers. Its major disadvantages are that we cannot investigate ferromagnetic materials and that the sample must be transparent for radiofrequency waves [1].

* Corresponding author.
E-mail address: robert.vajtai@rice.edu (R. Vajtai).

https://doi.org/10.1016/j.mtadv.2020.100084

Scanning electron microscopy (SEM) provides better resolution (nanometer scale) but only in 2D. To investigate 3D structure with SEM, the sample has to be sectioned, for example, with focused ion beam [2]. This destructive technique takes a lot of time and is limited to imaging a very small volume. Serial block-face scanning electron microscopy using ultramicrotomy allows imaging a bigger volume in an automated process, but it is not suitable for sensitive, brittle, or wet materials and the slicing can introduce serious artifacts [3].

3D imaging in a transmission electron microscope is called electron tomography. Transmission images of the sample acquired from at least a hundred different angles can be reconstructed into a 3D model of the sample. This is a very high-resolution (tens of nanometers) technique but only suitable for very small samples [4].

3D photoacoustic tomography is a non-invasive, non-destructive imaging technique with a millimeter resolution, where the contrast is based on the absorption of laser light [5].

X-ray can be used for imaging in many ways. The most common technique is traditional X-ray absorption imaging, where an X-ray beam passes through the sample and the transmitted radiation is detected to form a simple attenuation contrast image. The other possibilities include fluorescence X-ray tomography [6], dual-energy X-ray tomography [7], or phase-contrast X-ray tomography. Phase contrast is required in the case of low-density materials where attenuation contrast is not sufficient due to the small differences in the attenuation coefficients of materials. This technique requires a monochromatic beam and alterable sample to camera distances [8]. There is also a possibility to form a 3D map of the composition of samples with the X-ray diffraction method [9].

Computed tomography (CT) is a non-destructive 3D imaging technique based on the different X-ray attenuation of materials. Its non-destructive nature allows temporal investigation (some call it four-dimensional (4D) imaging, where the fourth dimension is time), and the examined samples remain unchanged, can be further investigated (even in situ), or can be put to use. Virtually no sample preparation is required, and thus it is suitable for samples that would lose their shape if sectioned manually. Samples remain intact during the measurement. In some cases, there is a need for contrast enhancement by contrast agents, but this usually does no harm to the sample. CT imaging allows multiscale investigation from millimeter resolution with clinical or industrial instruments to submicron resolution achievable using nano-CT. A broad variety of samples from biological materials to electronic devices can be investigated at a relatively high spatial resolution. Data obtained from CT scans can be the input of simulations or 3D models for additive manufacturing. The main limitations of CT are related to the high Z contrast necessary for good imaging quality. Low-Z materials and samples with low X-ray attenuation contrast are difficult to measure, whereas very high Z materials (e.g. metals) can introduce serious artifacts and worsen image quality. Some additional shortcomings are related to the very large data sets and lengthy image postprocessing procedures, the sample size–dependent resolution (in certain geometries), and the difficulties due to radiation-induced changes in the sample.

3D imaging modalities are compared in Fig. 1. Each technique has its own advantages and disadvantages (Table 1). Higher resolution typically means higher acquisition and operating cost. The use of low energy, non-ionizing radiation is cheaper, but its drawbacks are smaller penetration depth and inferior resolution. Some techniques allow examining a high variety of samples, but the increasing sample size is frequently paired with lower resolution, while higher resolution and better image quality often require longer measurement times. The use of non-destructive and non-invasive techniques is important for materials science applications, while the use of non-ionizing radiation can eliminate health hazards.

Imaging methods can be combined advantageously to eliminate certain drawbacks, for example, SEM can be combined with micro-CT to obtain 100-nm spatial resolution, which is worse than the resolution of SEM but is superior to that of most micro-CTs. The key idea here is to use the SEM electron beam to produce the X-ray radiation. This makes investigating the 3D structure possible in high resolution and non-destructively but only for small sample sizes [10]. It is also possible to capitalize on the complementarity of techniques, for example, CT and neutron tomography. Neutron tomography is an attenuation-based, non-destructive technique, with high contrast for low-Z materials with micrometer resolution. CT complements it well because the materials with high neutron attenuation have low X-ray attenuation. The methodological basis of the two techniques is the same [11,12]. However, neutron tomography has a restricted availability compared with CT because it requires a neutron source. Table 2 gives examples, where the combination of techniques is required to advance understanding in the field.

1.2. Micro-CT

1.2.1. Definition of micro-CT

Generally speaking, micro-CT is an X-ray tomography technique with (sub)micron resolution, using an X-ray tube with cone-beam geometry as a source and using a rotating sample holder. The history of X-ray imaging has begun in 1895 with the discovery of X-rays by Wilhelm Conrad Roentgen. In the 1970s, Sir Godfrey Hounsfield created the first computer tomograph for medical purposes [13]. With the advances in technology, high-resolution micro-CT was invented [14], followed by X-ray microscopy [15] and nano-CT [16]. Microcomputed tomography, computed microtomography, X-ray CT, X-ray microtomography, CT, X-ray microscopy, and microscopic CT are expressions where all refer to essentially the same technique. Micro-CT simply means high-resolution CT. With the decrease in focal spot size and increase in resolution, developers could achieve submicron resolution and started referring to devices capable of this high resolution as nano-CT [16]. After some time, with the use of synchrotron radiation and special X-ray optics, even better resolution (below 100 nm) became obtainable [17,18]. CTs equipped with X-ray lenses are often called X-ray microscopes. Stock [19] defines micro-CT as a high-resolution CT that can reach at least 50–100 μm resolution. Others place the resolution of micro-CT between 500 μm and 3 μm or even less [20].

Besides resolution, the second most apparent difference between medical CT and laboratory-based micro-CT is the measurement geometry. In medical scanners, there is a fixed patient table

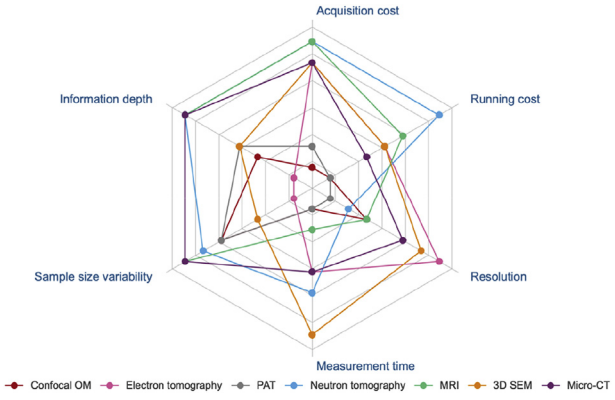

Fig. 1. Radar chart of the comparison of 3D imaging modalities. Axes are scaled in relative arbitrary units to facilitate qualitative comparison. 3D, three-dimensional.

Table 1
Typical advantages and drawbacks of the discussed 3D imaging modalities.

Characterization method	Pros	Cons
Confocal optical microscopy	Cost effective, non-destructive	Only transparent samples, limited penetration depth
Electron tomography	High resolution	Small sample size
Photoacoustic tomography	Non-destructive	Low resolution
Neutron tomography	Good contrast for low-Z materials	Costly, not readily available, highly trained operator required
Magnetic resonance imaging	Non-destructive, excellent contrast in soft tissues	Not suitable for ferromagnetic materials, radio frequency (RF) transparent sample needed
3D scanning electron microscopy	High resolution	Destructive, labor-intensive, sectioning required, not suitable for delicate samples
Computed tomography	Non-destructive, broad variety of samples	Costly, not ideal for high Z materials

Table 2
Examples of sample types requiring a combination of 3D imaging techniques.

Task	Ideal combination
Materials with highly different Z	CT + neutron tomography
Materials with highly different pore sizes	CT + SEM
Biological samples	CT + MRI
Samples with greatly varying feature sizes	CT + SEM

CT, computed tomography; SEM, scanning electron microscopy; MRI, ,magnetic resonance imaging.

with the detector and source rotating around it, whereas in typical micro-CT, the sample holder rotates around its own axis and the detector and source are fixed. Moreover, medical scanners tend to use fan-beam geometry, while in micro-CTs, cone-beam geometry is the most common. However, there are micro-CTs with fixed sample holders (e.g. for in vivo small animal imaging [21]), laboratory-based systems that use fan beams [22], and even parallel beam CTs (using synchrotron radiation) [23]. It is worth noting that besides the conventional X-ray attenuation–based approach, it is also possible to build other types of X-ray tomographs, for example, based on phase-contrast imaging [24].

Clearly, micro-CT is not a distinct, well-defined method, rather a diverse group of slightly different 3D X-ray absorption imaging techniques. For clarity, in this review, micro-CT will refer to devices capable of resolution better than 100 μm.

1.2.2. Basics of micro-CT

CT is a 3D non-destructive imaging technique based on the different X-ray attenuation of materials. The change in X-ray intensity upon passing through a material is described by the Lambert-Beer law as follows:

$$I = I_0 e^{-\mu x}$$

where I is the transmitted intensity, I_0 is the incident X-ray intensity, μ is the linear attenuation coefficient (LAC), and x is the thickness of the sample. The LAC depends on the density and atomic number of the material and the applied X-ray energy.

The X-ray beam passes through the material, where – depending on the LAC – some of the X-ray photons are absorbed. Transmitted photons are detected by a detector (e.g. a high-resolution charge-coupled device (CCD)) placed on the opposite side of the sample, and thus a single 2D attenuation map (shadow projection) is obtained. Because the sample is rotated (in 180° or 360°), the shadow projection image is acquired in numerous different angles. The detailed 3D structure of the samples is reconstructed from these hundreds (or even thousands) of images with the help of image reconstruction algorithms, most frequently some modified versions of Feldkamp's back-projection algorithm [25]. After reconstruction, an image postprocessing step is required to analyze the results. For most calculations, an image segmentation step is needed to convert the original greyscale attenuation image into a 2-bit data set. In a lot of cases, the analysis of the images is more time consuming than the image acquisition itself because of the huge size of the data set.

The X-ray source in laboratory-based micro-CTs is usually an X-ray tube with cone-beam geometry. In this case, geometric magnification occurs, which highlights the importance of the source to object and source to detector distances. The magnification (M) can be calculated as follows:

$$M = \frac{SDD}{SOD}$$

For the same comparability and reproducibility, the Hounsfield unit (HU) was introduced, which is also termed as the CT value. The HU value of water is 0 and that of air is −1000. The HU value of a material can be calculated as follows:

$$HU = 100 * \frac{\mu - \mu_{water}}{\mu_{water} - \mu_{air}}$$

where μ is the LAC of the sample, μ_{water} is the LAC of water, and μ_{air} is the LAC of air.

The image quality is influenced by the voltage and current of the X-ray tube. Other important parameters are the rotation rate, the exposure time, and the quality of the sample. The detector system and the applied reconstruction algorithm can also affect the quality. For optimizing the image quality, the proper mounting of the sample is crucial because even a small displacement of the sample can introduce serious artifacts.

1.2.3. Resolution – limits and possibilities

The resolution can be calculated with the following equation.

$$R = \frac{d}{M} + \left(1 - \frac{1}{M}\right) * s$$

Here, R is the size of the voxel, d is the resolution of the detector, M is the magnification, and s is the size of the focal spot of the source. With different types of CTs (e.g. industrial, medical, micro-CT, nano-CT, X-ray microscopy) allowing different sample size and resolution, there are multiscale opportunities with CT. The typical resolution of medical, industrial, micro-CT, and nano-CT scanners is 70–1000 μm, 5–150 μm, 1–100 μm, and around 0.5 μm [26], respectively. With X-ray microscopy, resolution less than 100 nm is also achievable.

The resolution improves with decreasing pixel size but only to the point where the pixel size reaches the diameter of the focal spot. Although the pixel size could be smaller than the focal spot in theory, the actual resolution will not improve [27]. The size of the focal spot increases with the applied X-ray tube power. In systems with cone-beam geometry, the effective resolution of micro-CT images depends greatly on the size and shape of the sample.

Cylindrical samples are optimal for fixed X-ray source + fixed detector geometries because imaging artifacts are unavoidable for asymmetrical sample shapes. Synchrotron X-ray sources can provide parallel, monochromatic, high flux beams for superior image quality.

Fig. 2 presents an overview of the operating principle of X-ray tomography, the characteristic length scales of the currently available CT methods, the main do's and don'ts of micro-CT sample choices, and most important perturbations compatible with in situ micro-CT measurement.

Similarly to many characterization methods, temporal and spatial resolution is inversely related in a micro-CT experiment. However, unlike most techniques (e.g. electron microscopy, spectroscopies, X-ray diffraction, and so on), micro-CT inevitably involves the physical movement of the sample. High spatial resolution is only achievable by using a large number of slices that requires many sample motion steps. To avoid motion artifacts (refer following paragraphs), it is necessary to wait some for time after each rotation, and even very bright X-ray sources (e.g. synchrotron radiation) are unable to fully compensate for the time lost here. Therefore, very fast, quasi real-time measurements lack the high quality and resolution of standard micro-CT imaging and vice versa: measurements with good resolution can take several hours. It is an accepted practice in the field to circumvent this by first taking high resolution, high quality images to evaluate the detailed structure of the sample and then acquiring a series of lower quality 'fast' images to monitor ongoing inner processes or changes in the investigated systems in situ.

1.2.4. Imaging artifacts

Many factors can introduce artifacts at various stages of the micro-CT measurement, but most of these artifacts are normally corrected in the image reconstruction step to some extent. The samples have intrinsic attributes that can lead to imaging errors. For example, wet samples can suffer shape alterations caused by drying during imaging. This can be prevented by the airtight sealing of the samples. High Z contrast is an important criterion for high-quality X-ray imaging. Too high contrast, however, is apt to cause streak artifacts. This effect mainly appears parallel to large areas of flat surfaces; therefore, it is advisable to avoid such sample geometries.

Very light and thin samples can shift because of the rotating motion of the sample holder, resulting in so-called motion artifacts. These can be avoided by adding a short waiting period after each rotation step. Inadequate sample mounting and any off-axis movement of the sample holder besides the rotating motion (e.g. wobbling of the rotation stage) also causes artifacts. These motion artifacts can be corrected if reference images are taken to monitor the incidental movements. The importance of appropriately small rotation step size must be emphasized because undersampling is one of the main causes of imaging artifacts. The more asymmetric the sample, the more issues are caused by undersampling. For an accurate reconstruction of the sample, the precise definition of the rotation axis is indispensable; the incorrect definition of the reconstruction center leads to the appearance of tail-like artifacts.

Beam hardening appears when polychromatic X-ray radiation is used. Because the softer components of the radiation are absorbed more easily, the attenuation cannot be described by a linear coefficient. This effect worsens with increasing sample thickness and can be eliminated by using appropriate filters. The most commonly used cone-beam geometry itself is a source of error because in this setting only a single slice (the middle one, aligned with the cone axis) is imaged perfectly. In this plane, the imaging is practically performed by a fan beam. Consequently, only the middle line of the detector gets information exclusively from one sample slice and all the others receive combined information from many slices. Therefore, the reconstruction of these off-axis slices is more uncertain. This effect worsens, the further away we get from the middle slice.

Contamination of the detector surface or the failure of even a single detector element can introduce ring artifacts, thus causing inferior image quality. Ring artifacts are routinely corrected during

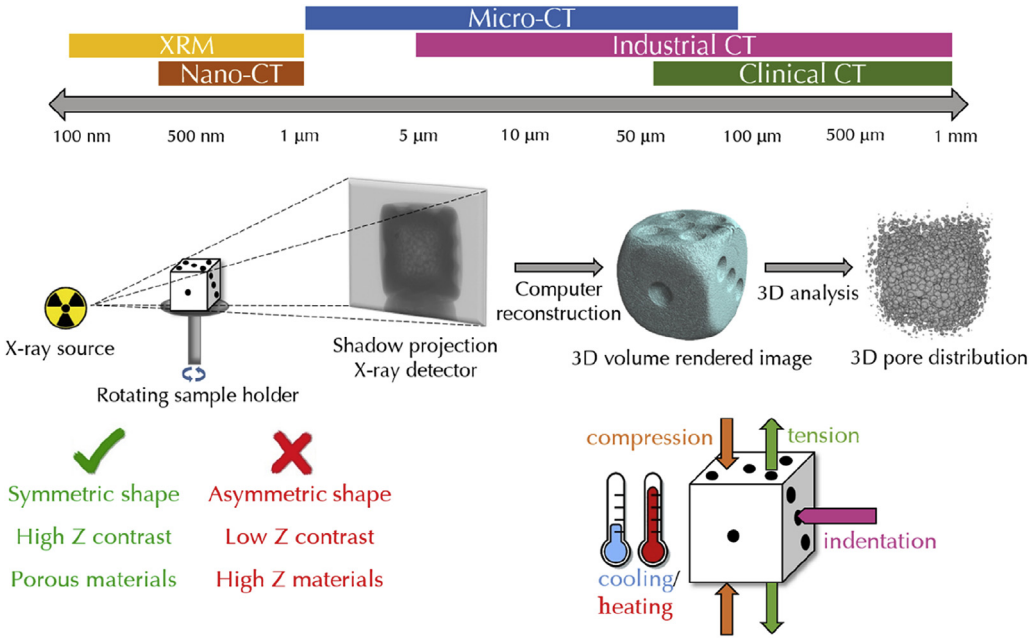

Fig. 2. A micro-CT cheat sheet prepared using actual images of a commercial dice recorded in the authors' laboratory. In situ measurement possibilities are limited only by innovativeness in measurement cell design. Thus, custom-made equipment for, for example, electrical testing, catalytic reactions studying wetting/wicking phenomena is also used. CT, computed tomography.

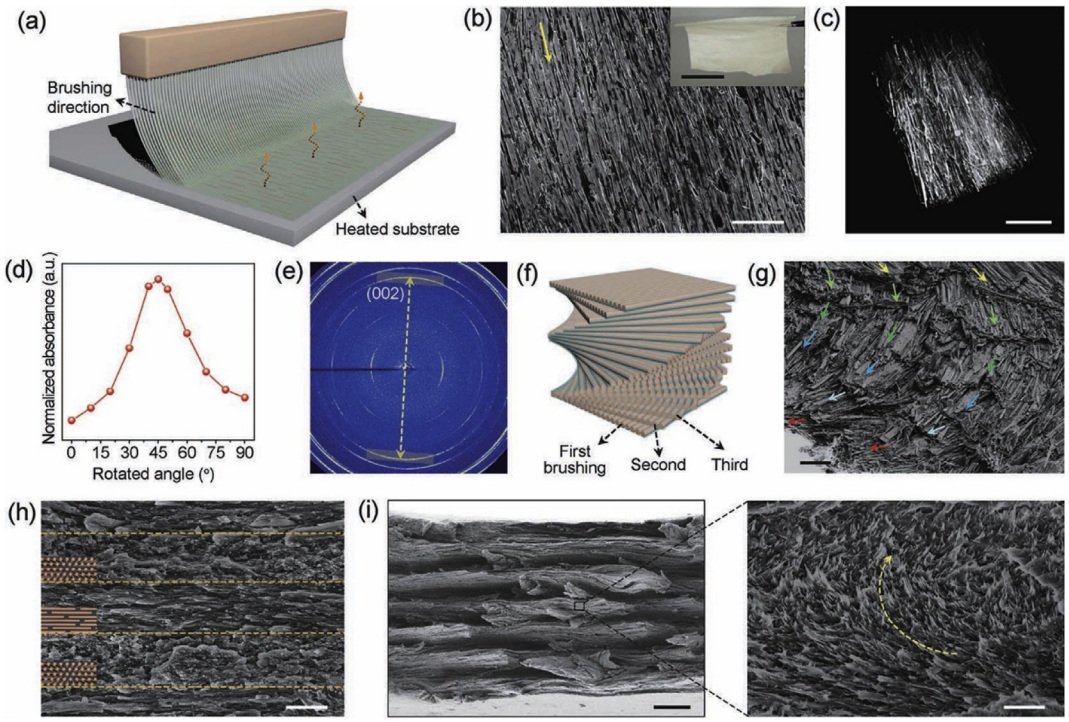

Fig. 3. Brushing-induced assembly for flexibly aligning 1D micro/nanofibers and structural characterizations. (a) Schematic illustration of the brushing-induced assembly method for aligning Hydroxyapatite (HA) microfibers on a heated substrate. (b) SEM image showing the surface of the HA-SA film with unidirectionally aligned HA microfibers; the yellow arrow denotes the brushing direction. The inset is a digital image of the film. Scale bars: 50 μm and 5 cm (inset). (c) Nano-CT image of the HA-SA film with unidirectionally aligned HA microfibers. Scale bar: 10 μm. (d) Absorbance curve of the HA-Sodium Alginate (SA) film with unidirectionally aligned HA microfibers, showing the typical peak value due to the birefringence effect. Note that the angle values labeled on the abscissa only represent the rotated angle range (0°–90°) of aligned film and do not indicate the real-time deviation angle between alignment direction and polarizing directions. When the aligned film was rotated to around 45°, the peak value of absorbance appeared. Actually the deviation angle between alignment direction and polarizing direction (one of the two polarizers) was around 0° rather than 45° at this moment, demonstrating the largest absorption. (e) X-ray diffraction pattern of the HA-SA film with unidirectionally aligned HA microfibers. (f) Schematic illustration showing the programmed and continuous brushing procedure with each brushing process twisting at a predefined deviation angle for designing a complicated twisted plywood structural film. (g) Cross-sectional SEM image of the obtained HA-SA film prepared by the programmed and continuous brushing procedure, showing obviously twisted plywood structure. Various colored arrows represent gradually twisted microfiber lamellae. Scale bar: 20 μm. (h) Cross-sectional SEM image of the xonotlite nanowire (20 wt%)-SA composite film prepared by the continuous and crossed brushing procedure, showing ~90° cross-stacked xonotlite nanowires in an SA matrix. Scale bar: 2 μm. (i) Cross-sectional SEM images of the xonotlite nanowire (20 wt%)-SA composite film prepared by the programmed and continuous brushing procedure with each brushing process twisting at a predefined ~30° deviation angle, showing distinct periodically helical structure. Scale bars: 20 μm and 2 μm. SEM, scanning electron microscopy.

reconstruction. A lot of imaging errors originating from the imperfections of the X-ray source or the detector can be corrected by white and dark flat-field correction (images taken without the sample in the field of view or with the source turned off). Phase-contrast phenomena are useful in some cases, but when they appear unintentionally, they are considered artifacts. They appear only in the case of monochromatic radiation and manifest in the sharpening of edges [28].

1.2.5. In situ investigations

The non-destructive nature of micro-CT makes it suitable for temporal investigations (time-lapse imaging or 4D micro-CT). For example, the effects of corrosive environment or different weather conditions on structural materials can be investigated or changes during the lifetime of an electronic device can be monitored. This type of investigation is called postmortem tomography: a sample is exposed to external impacts and then measured by micro-CT. Repeated measurements are carried out on either different sample pieces or on a single piece measured repeatedly over time. If the sample is removed from the CT instrument to apply changes, the method is called ex situ tomography, whereas in situ micro-CT refers to carrying out the investigation without the need to remove the sample by using specially designed testing stages. This facilitates the identification of the exact changes in the structure and even allows individually monitoring the changes occurring in a single pore or in a predefined part of the sample.

In situ micro-CT measurements provide unique possibilities in many fields, especially in material design and development. The two main types of in situ investigations are interrupted and continuous [29]. In case of interrupted in situ tomography, the sample is exposed to a certain impact, then for the time of the measurement, the sample is 'frozen' into this state, after which it can be exposed to changes again. For example, the sample is compressed with a certain force and a measurement is performed, afterward the force is increased and another CT measurement is performed, and this is repeated for several cycles. Mechanical tests can be compressive or tensile measurements, as well as indentation or bending tests. Changes in shape, size, and porosity, as well as crack initiation and propagation as a result of mechanical impact are readily investigated this way. One of the main advantages of in situ micro-CT is its ability to provide information about the exact changes in the structure. This eliminates the need for additional characterization by other methods and thus reduces the required sample size. Moreover, it is also possible to follow the exact changes a specific external force has on structural features and determine if the sample deforms uniformly or not. Interrupted in situ

investigations can also be used with a gradual thermal profile to determine shrinkage, thermal expansion, or freezing characteristics.

In continuous in situ tomography, processes are monitored in quasi real time. This assumes a short image acquisition time because even slight changes in the structure during measurement can introduce serious artifacts upon the reconstruction and thus decrease the final image quality. Fortunately, software post-processing offers an opportunity to compensate for artifacts caused by motion and improve the quality of the reconstructed images, and this makes investigating dynamic processes possible [30]. Synchrotron X-ray sources are particularly well suited for continuous in situ tomography because the high photon flux reduces micro-CT image acquisition times to seconds. This allows the in operando investigation of electrochemical cells, batteries, fuel cells, and other electronic devices. In situ flow micro-CT systems offer insight into oil recovery from rocks or gas storage capacity assessment.

2. Applications

CT imaging traditionally served medical purposes, but with the spread and improvement of the technique, other applications came into view. Medicine, food chemistry, dentistry, geoscience, life sciences, petroleum geology, scaffolds, building materials, nanotechnology, additive manufacturing, and tissue engineering are just a few examples of the possible fields of micro-CT application.

The primary information from micro-CT is the difference in X-ray attenuation, and the resulting direct quantitative outcome is the absorption map (2D or 3D) that can be enhanced by postprocessing. The presence of pores, cracks, and structural errors can be verified, and the 3D inner structure of samples can be investigated. In this sense, micro-CT is a qualitative diagnostic tool. However, quantitative data are also obtainable: porosity, pore size distribution, connectivity of pores, shape, size and orientation of individual pores/objects/phases/regions, spatial distribution, volume fraction, and other density variations can be determined [31].

While appreciating the visual stimulation of 3D reconstructions, it is important to remember that they are based solely on X-ray attenuation contrast. Application field–specific meaning is bestowed upon the differences only later, and vastly different interpretations of the same observation are possible depending on what the images actually represent. For example, pores in bricks are normal and important for thermal insulation and freeze tolerance, while identically sized pores in a metallic car part can reveal severe manufacturing errors. Therefore, it is with the critical interpretation of the obtained information that real material science in micro-CT begins.

2.1. Bio(inspired) materials

The term ‘biomaterial’ is a very generic one. It can refer to any material that is designed to interact with a biological system (often as part of a medical treatment). When materials science turns to nature for ideas to create new types of materials and improve the quality and applicability of existing ones, ‘bioinspired’ materials are the result; when inspiration turns into direct plagiarism, we create ‘biomimetic’ materials. Micro-CT investigation can provide valuable information about each class. For example, micro-CT is a very capable tool for investigating bone formation/regeneration around implants. Cohen et al. [32] examined the bone growth around a solid implant and the bone penetration into a porous implant in the rabbit femur. X-ray imaging was also used successfully to reveal inferior screw stability in an implant [33] and in revealing the 3D structure of the bone to possibly create a superior bone-mimicking material [34]. Several features of porous bioceramic scaffolds were compared with the bone tissue by micro-CT, and a metric was created for the comparison of scaffolds to the bone in an attempt to help the fabrication of bone-like ceramics [35]. Bioscaffold design and investigation by micro-CT was recently reviewed by Cengiz et al. [36]. Some other notable examples of micro-CT applications at the interface of the live world and materials science include dentistry (where it can help improve dental fillings, crowns, and implants) and artificial organ design (assisting cardiovascular engineering and bioinspired design) [37].

Biomimetic materials are designed to replicate biological phenomena for scientific purposes. To truly mimic the beneficial features of various biological systems, it is imperative to learn their 3D structure. Fig. 3 gives a representative example for creating a biomimetic twisted plywood structural material [38], and the recent work of du Plessis and Broeckhoven [39] reviews the biomimicry aspects of micro-CT in detail.

Micro-CT application examples are plenty for functional biomimetics as well. The morphological characterization of a beetle wing was helpful in creating artificial insect-sized wings for micro air vehicles [40]. X-ray imaging turned out to be particularly useful in mapping the microstructure of the wings, their vascular network, the flight muscles, and the wing joints [41]. Bioinspired artificial body armor was created by the micro-CT study, reverse engineering, and 3D printing of an extinct armadillo-like mammal species [42]. Data obtained from the micro-CT investigation of tree joints were used to create biomimetic aerospace composite joints with improved mechanical properties. The study showed that there is a porosity difference between the parts experiencing different levels of stress in tree joints. The fabricated biomimetic joints tolerated 27% higher bending load without any adverse effects in tensile or compressive strength [43]. In 2016, Frank et al. [44] have suggested a protocol for biomimetic design and demonstrated it by 3D printing a sediment sampler inspired by the micro-CT–based 3D model of the jaw of a sea urchin (also known as Aristotle's lantern). Later, a bionic hydraulic system was designed on the basis of a micro-CT–based 3D model of the joints in spider legs [45], and highly sensitive and directional acoustic sensors were inspired by the micro-CT–derived microstructure of the hearing organ of *Ormia ochracea* flies [46].

Interestingly, in situ micro-CT is also applicable in functional biomimetic material research. In 2018, Wang et al. [47] reported the in situ compression stress testing of pomelo peel and used the micro-CT insight into its hierarchical structure to understand its outstanding stress resistance, damping capability, and energy absorption properties.

2.2. Structural materials

Micro-CT is widely applicable for the characterization of structural materials both on a small scale, such as 3D printed objects, and on bigger samples, such as building materials, for example, cement or concrete. It is particularly well suited for investigating fatigue-induced structural changes. Chowdhury et al. [48] determined the micro-mechanisms of damage in carbon-carbon composites for application in the aerospace industry. The micro-CT evaluation helped them understand the crack advancing mechanism, which is an important step in improving the composites and finding the ideal microstructure [48].

Porosity analysis is one of the most popular applications of micro-CT as it yields both qualitative (shape, size, distribution) and quantitative (porosity, connectivity) information about the open and closed pores in micrometer scale. This is of pivotal importance for structural materials where even a slight change in porosity or an asymmetrical pore distribution can lead to huge differences in

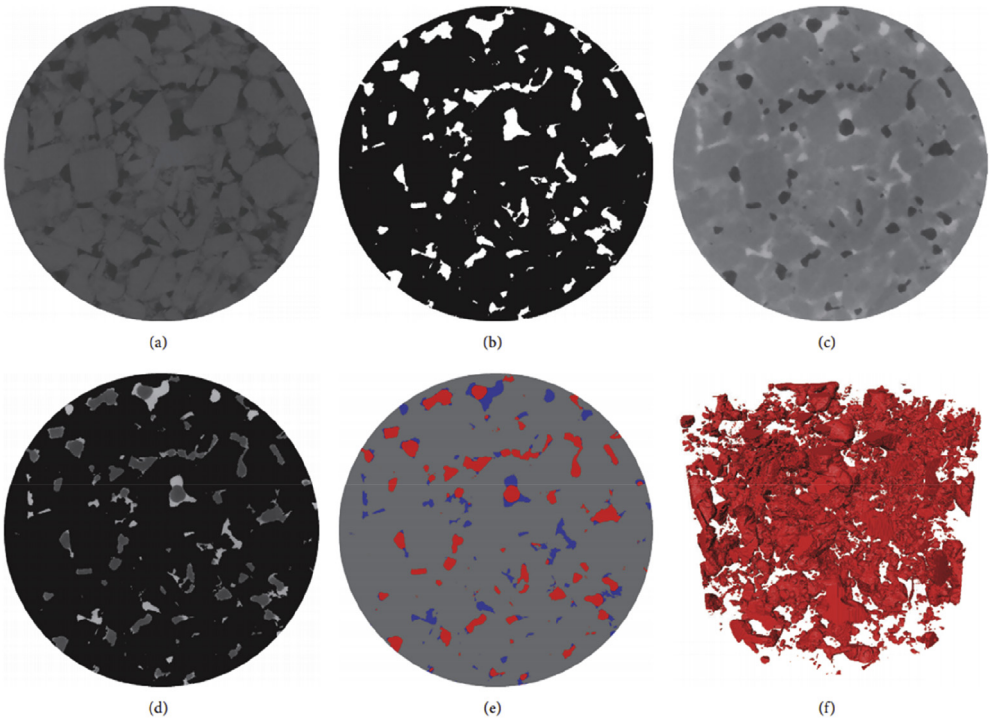

Fig. 4. Horizontal cross-sectional slices through the plug (diameter = 1400 voxel) and the image processing workflow of wet and dry images taken during the water-wet plug flooding (slice number = 135, 24.92 mm from the inlet). (a) Filtered dry reference image; (b) pore map obtained from the filtered dry image, where the pore is transparent and the grain is black; (c) filtered wet image, where the darkest phase is oil, the light gray phase is brine, and the intermediate phase is solid particle; (d) combined wet image, where oil, brine, and the solid are dark gray, light gray, and black, respectively; (e) segmented wet image (brine: blue; oil: red; and grains: gray); (f) three-dimensional rendering of the oil phase. Brine and rock are transparent for effective visualization. Copyright © 2018 Junjian Li et al.

mechanical properties and behavior of the materials. Failure visualization can help determine the cause of the failure and improve the material properties, and micro-CT images can be inputs for 3D simulations, for example, stress distribution and possible failure site modeling [49]. Filler aggregation and fatigue behavior (crack formation and propagation) of carbon black (CB) or silica-reinforced filled rubber materials were also visualized successfully by micro-CT [50].

The discontinuities, pores, fractures, and inaccuracies occurring during the 3D printing process are typically in the micrometer-millimeter scale, which makes them very well suited for micro-CT examination. Moreover, micro-CT characterization is a valuable element of method development in additive manufacturing; it helps in the fine tuning of the printing parameters.

Besides the most common polymers, Polylactic Acid, Acrylonitrile Butadiene Styrene, Polyethylene Terephthalate, Polycarbonate (PLA, ABS, PET, PC), ceramics, concrete, and even metals [51] can be 3D printed today, and they are all examinable by micro-CT. In an interesting recent study, Wu et al. [52] designed and fabricated gradient porous Ti−6Al−4V specimens by 3D printing (electron beam melting) and studied their mechanical properties. These materials can be used as implants; they have regions with differing porosities to endure the differing stress levels experienced by various regions of bones. With the help of micro-CT, they could find the interface mismatches, redesign the specimens, and thus improve their mechanical strength [52]. We refer to the review by du Plessis et al. [53] for the in-depth coverage of the additive manufacturing topic.

Cement and concrete are among the most researched building materials. Studies focusing on the investigation of these materials with the help of micro-CT are abundant, and specific reviews are available [54–56]. The most important micro-CT derived structural parameters are porosity, density, and phase distribution. The resulting images can be used as input for 3D simulations [20], and temporal investigation allows the monitoring of damage evolution as well.

A key issue in building material development is strengthening the materials while lowering their density, and lightweight cement foams are good candidates for this. Their fracture initiation and propagation mechanism was recently investigated by in situ micro-CT [57] that revealed a clear relationship between the appearance of cracks and the presence of standard K15 and K46 microspheres.

The non-destructive nature of micro-CT is particularly valuable in building material characterization because it makes examining the same sample repeatedly over the time possible; thus, we can follow the changes occurring during, for example, cement hydration, binding/curing/aging of the concrete, or freeze-thaw cycles in mortars [58]. Micro-CT can be used to differentiate between cement paste and corrosion products close to a rebar in reinforced concrete [59], and the damage caused by sulfate attacks in concrete can also be visualized [60].

2.3. Energy and environment

2.3.1. Porous rocks

Micro-CT studies are extremely important in energy and environment applications because these rely often on understanding the 3D pore structure and fluid migration dynamics in solid objects. For example, images from a time lapse micro-CT study performed in a high pressure in situ flow cell could be used as input for the simulation of capillary CO_2 trapping in sandstone relevant for geological storage development [61]. The effect of injection pressure on gas storage in sandstone gas saturation was investigated by micro-CT using the differences between the X-ray absorption characteristics of nitrogen gas and water during displacement in the pores [62]. In hydraulic fracturing for geothermal energy

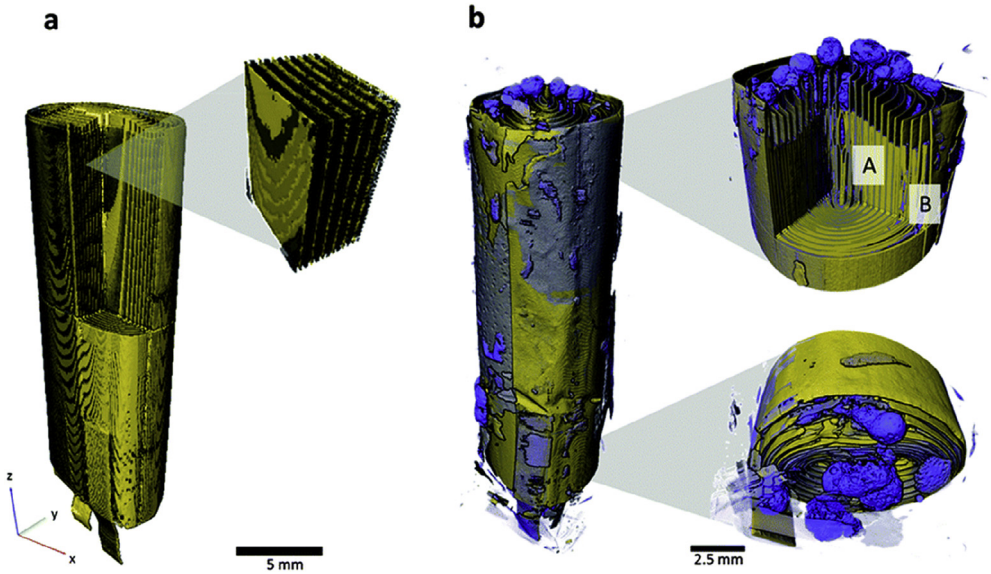

Fig. 5. (a) 3D reconstruction of the pouch cell in its fresh state. The $LiCoO_2$ electrode is displayed as gray, and the copper current collector and tabs are shown in yellow. (b) 3D reconstruction showing the pouch cell after overcharge-induced thermal runaway. Copper and $LiCoO_2$ phases are labeled as yellow and aluminum is shown in blue. Samples were taken from regions A and B for further analysis using micro-X-ray CT. Republished with permission of Royal Society of Chemistry, from Investigating lithium-ion battery materials during overcharge-induced thermal runaway: an operando and multi-scale X-ray CT study, Donal P. Finegan, Mario Scheel, James B. Robinson, Bernhard Tjaden, Marco Di Michiel, Gareth Hinds, Dan J. L. Bretta, Paul R. Shearing, 18, 2016; permission conveyed through Copyright Clearance Center, Inc. 3D, three-dimensional; CT, computed tomography.

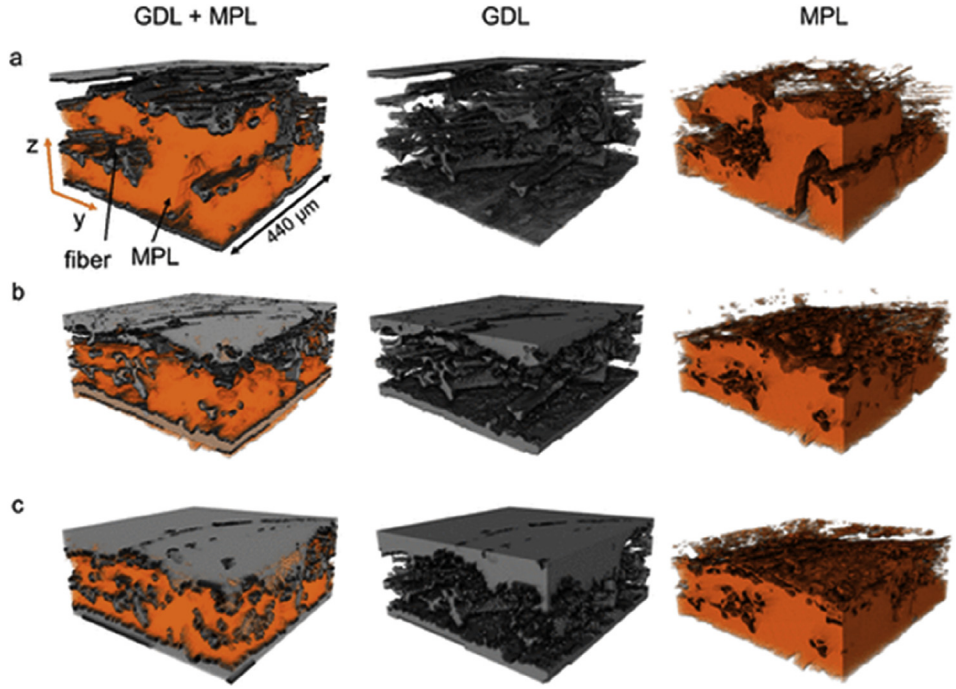

Fig. 6. Volume-rendered SGL 29BC gas diffusion medium (GDM) showing microporous layer (MPL), gas diffusion layer (GDL), and void with separate renderings of individual components at (a) 0%, (b) 34%, and (c) 41% compression. The z-axis indicates the GDM through-plane direction; the y-axis corresponds to the in-plane direction. Reprinted with permission from Robert W. Atkinson, III, Yannick Garsany, Benjamin D. Gould, Karen E. Swider-Lyons, and Iryna V. Zenyuk ACS Applied Energy Materials 2018 1 (1), 191−201 https://doi.org/10.1021/acsaem.7b00077. Copyright (2018) American Chemical Society. MPL, microporous layer; GDL, gas diffusion layer.

extraction, the micro-CT investigation of the microstructure and fracture propagation in a high temperature and high pressure environment has led to the better understanding of the underlying mechanisms [63].

It is possible to conduct in situ micro-CT studies on drill core samples and model rock formations to assess oil recovery options, survey fractured hydrocarbon reservoirs, investigate the remaining oil saturation, study the impact of spreading, and perform flow experiments [64]. Understanding the multiphase flow inside realistic rock structures is crucial for oil recovery efficiency maximization. Micro-CT was used successfully for understanding fluid distribution in sandstone at different saturation states. 2D

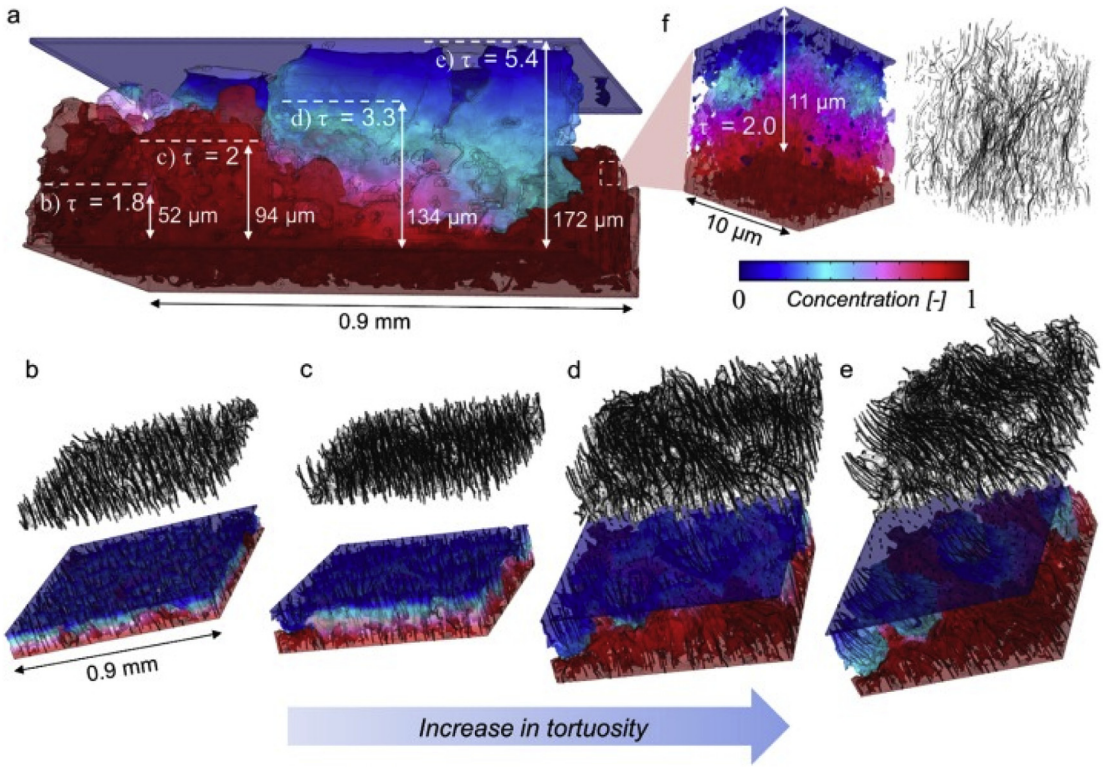

Fig. 7. Study of tortuosity as a function of sample thickness with micro-CT starting from the MPL interface, where (a) shows full sample thickness and each subdivision. (b–e) Samples of varied thicknesses. (f) Mesoscale tortuosity obtained with nano-CT. Reprinted from Applied Catalysis B: Environmental, Vol. 237, Alexey Serov, Andrew D. Shum, Xianghui Xiao, Vincent De Andrade, Kateryna Artyushkova, Iryna V. Zenyuk, Plamen Atanassov, Nano-structured platinum group metal-free catalysts and their integration in fuel cell electrode architectures, Copyright (2018), with permission from Elsevier. CT, computed tomography; MPL, microporous layer.

saturation maps were made from simple radiographs during flooding, and after each sequence, 3D X-ray imaging was performed [65]. In a study performed on the porous rock – brine – oil ternary system, the oil cluster dynamics were revealed by micro-CT during drainage and imbibition. The authors have found that 'wettability, pore size distribution, and pore connectivity have a strong impact on fluid saturations, cluster morphologies, and potentially cluster size distributions' [66]. Fig. 4 presents characteristic horizontal cross-sectional slices obtained by micro-CT in this study.

2.3.2. Energy storage

Micro-CT imaging allows the investigation of the complex inner structure of energy storage devices in high detail from the smallest batteries to whole fuel cells and can help in quality control and the detection of faulty parts. Beyond simple 3D imaging, micro-CT holds a greater advantage because devices can be investigated in operando conditions over time. This is typically made possible by using synchrotron X-ray sources where the high flux of the synchrotron source allows 3D image acquisition in seconds [67].

The performance loss of energy storage devices over time is due to changes in their microstructure. Therefore, visualizing their microstructure in 3D – preferably repeatedly over time or in operando condition– is crucial in their development. Originally synchrotron radiation was needed for electrical device characterization but advances in laboratory-based micro-CT systems rendered them more and more suitable for such work. Nowadays, the main areas of investigation in the field of energy storage are batteries (especially Li-ion) and fuel cells, mainly polymer-electrolyte and solid oxide fuel cells (SOFCs) [68].

Micro-CT was successfully used to investigate inhomogeneities in the microstructure of Li-ion battery electrodes to determine their role on the battery performance [69]. The method is particularly useful to visualize the effects of extreme conditions. For example, nail penetration tests were carried out to investigate the short circuits and the changes in the 3D battery structure [70]. In another work, a Li-ion 18,650 battery cell was exposed to axial compression tests to understand its failure mechanism. The obtained micro-CT data were in good agreement with the finite element model simulations [71]. One of the early works in the field is that of Finegan et al. [72] who studied the overcharge-induced thermal runaway in Li-ion battery materials by in operando CT and facilitated the even better understanding of the failure process by postmortem micro-CT scans (Fig. 5).

Micro-CT also proved its merits in the characterization of Li-iron phosphate batteries postmortem after high rate cycling [73] and helped optimize the electrode microstructures of Li-sulfur battery electrodes [74]. The depletion region in the sulfur composite cathode was very clearly observable even after 2 cycles at 0.15 mA cm^{-2}.

An important non–Li-ion battery–related micro-CT application is the optimization of the absorptive glass mat separator, a pivotal component of valve-regulated lead acid batteries [75]. Shukla et al [76] have recently used micro-CT to develop a comprehensive, predictive model of hydraulic tortuosity for this important field.

2.3.3. Energy conversion

The performance of fuel cells is largely determined by the microstructure and spatial distribution of components in the gas diffusion layer (GDL), the microporous layer, and the catalyst layers [77]. Each of these components can be studied by micro-CT [78] even though in operando fuel cell design can be challenging [79].

Table 3
An overview of commercially available benchtop micro-CT instruments. Specifications are taken from the brochures available from the manufacturer's homepages unless noted otherwise.[a]

Instrument	Dimensions (mm)	Weight (kg)	Max. tube voltage (kV)	Voxel size (μm)
Bruker Skyscan 1273	1250 × 815 × 820	400	130	<3
Procon CT-Compact[b]	Not stated explicitly	500	160	3.5
Rigaku CT Lab HX	980 × 700 × 580	380	130	2.2
Sanying nanoVoxel-1000	900 × 500 × 650	500	110	2
Shimadzu inspeXio SMX-90CT Plus	830 × 501 × 587	250	90	Not stated explicitly

[a] Well-known full-scale CT manufacturers GE, Siemens and Yxlon do not feature any comparable benchtop units on their respective homepages as of May 8, 2020.
[b] Data collected from secondary sources because the datasheet directly available from the homepage of the manufacturer does not cite specific values.

The effect of GDL microstructure on mass transport in a proton exchange membrane fuel cell was successfully investigated by in situ micro-CT compressive tests [80]. In the work illustrated in Fig. 6, the gas diffusion media of a polymer electrolyte fuel cell (PEFC) were compressed in a micro-CT and the changes in the microstructure and the performance were monitored [81].

In another work, to complement the results of oxygen concentration measurement, 3D X-ray microanalysis was conducted on the diffusion media of a PEFC [82].

Micro-CT is very well suited to monitor water distribution inside a GDL that affects the performance of PEFCs to a large extent [83]. Water formation could also be observed in alkaline exchange membrane fuel cells (platinum group metal−free catalyst) in operando conditions [84]. The main finding of these studies was that large pores in the GDL are undesirable because of water pooling and blocking of active sites [85]. The wetting and evaporation of a carbon cloth type GDL by aqueous alcohol mixtures was systematically studied very recently. Micro-CT was crucial in this work to link the observed behavior to GDL structural features [86].

Fuel starvation caused degradation can be an important limiting factor of the lifetime of fuel cells. Micro-CT measurements have recently helped Yezerska et al. [87] to determine the influence of starvation of the thickness of the cathode and the anode catalyst layers in high-temperature proton exchange membrane (HT-PEM) fuel cells.

The effects of hot-pressing parameters on the microstructure of PEFCs were investigated. Micro-CT combined with electrochemical measurements helped in the development of optimized membrane electrode assemblies (MEAs) [88], and Serov et al. [89] have uncovered the relationship between MEA thickness and tortuosity as shown in Fig. 7.

Another notable multiscale approach was published by Meyer et al. [90] who advantageously combined micro-CT with nano-CT, transmission electron microscopy, and helium-ion microscopy to investigate PEFC MEA structure.

A good example of micro-CT studies focused on fuel cell catalysts was published by Roy et al. [91] about in situ and in operando MEA measurements with integrated nickel-copper catalysts supported on CB. From the CT results, the hydrophobicity of the NiCu state in the NiCu/CB system was determined that has led to improved water distribution and could explain the high catalytic activity of the composite [91]. Cracks in the catalyst layer, the results of degradation processes, and mechanical defects can also be visualized by postmortem (ex situ) micro-CT MEA analysis [92].

As for non-polymeric fuel cells, it is worth mentioning that a SOFC anode with hierarchical microstructure was characterized by a multiscale 3D X-ray tomography method to help and understand its operation mechanism. The unique microstructure led to a 250% increase in the mass transport and a 2−3 orders of magnitude increase in the permeability. These results can help to design and optimize hierarchical electrode microstructures [93]. Micro-CT has helped in finding the connection between performance loss and changes in microstructure (carbonate scale deposition) in microbial fuel cell biocathodes that were measured were in different stages of operation [94].

It would be excellent to investigate the layered structure of solar cells by micro-CT to observe, for example, perovskite deterioration or transport layer inhomogeneities. Unfortunately, the typical solar cell layer thickness tends to be too thin for micro-CT to resolve correctly, especially because the image quality is worsened by artifacts originating from the highly asymmetrical shape of the layer. Nevertheless, it seems reasonable to anticipate progress in this field in the next few years.

2.3.4. Filtration

Micro-CT is very useful in the design of efficient filters and in improving filter models for more accurate simulations. For example, it revealed local changes in porosity through the whole thickness of a fibrous filter and captured the structure-dependent behavior of deposits: these do not leave the filter, rather they gradually move to the deeper regions [95]. It was also possible to study the effects of microstructure on aerosol deposition in high efficiency particulate air (HEPA) filters [96], assess liquid distribution in the filter during liquid aerosol filtration, and uncover the effects of filtration velocity on clogging [97]. Water filtration membranes are also accessible for micro-CT analysis. A porous membrane with well-defined microstructure was designed and monitored by micro-CT. It offered improved antifouling ability because of the site-specific silver decoration of the polyethylene ionomer membrane [98].

3. Outlook

It is without doubt that micro-CT is becoming a mainstream materials science and material development tool today. Its chief merits are its non-destructive nature that allows temporal investigation, the relative ease of combining 3D structural characterization with real-time in situ perturbations, and the natural link between computational materials science and CT-based models. We can expect further development in the following directions. The technical improvement of the hardware (e.g. more powerful and brighter X-ray tubes, better detectors) will bring about better resolution and shorter exposure times, thus narrowing the gap between synchrotron based and laboratory-based units. This will be particularly relevant for more widely accessible in operando studies.

The spreading of benchtop laboratory CT units is not hindered by unmet technological challenges, as adequate small-size X-ray sources, detectors, and precision sample stage mechanics are already available. Rather the main limiting factor appears to be the physical size of the unit. Lead plating is necessary to protect the operator from X-ray exposure, and a heavy base plate (e.g. granite slab) is required for mechanical precision. State-of-the-art benchtop CT units are only slightly larger in volume than an upmarket UV-Vis spectrometer but they are much heavier (Table 3.). Note that the performance metrics of the units listed in Table 3 are clearly inferior to those of 'full size' micro-CT instruments that tend to have

the volume of a large wardrobe, weight 2–4 tons, have X-ray tubes going above 190 kV, and offer submicrometer resolution. The footprint of current benchtop micro-CT systems is unlikely to decrease significantly in the near future. However, we can expect improvements in X-ray tube voltage and resolution, and thus the benchtop micro-CTs of the near future are likely to be very capable laboratory-based units – it is just that high performance and true portability in a single package are not in sight yet.

The smallest commercially available CT scanner today is the ProCon CT-Portable. Measuring 350 × 300 × 230 mm and weighting 20 kg, this unit can be carried by a single person; therefore, its portability is unquestionable. However, the severe trade-offs in the X-ray tube voltage (50 kV) and resolution (voxel size <18 μm) narrow the materials science applicability of this unit mostly to the non-demanding 3D imaging of soft materials.

Software developments will improve automated image analysis including advanced thresholding by artificial intelligence, reduce analysis errors introduced by the human operator, and provide workarounds for eliminating image artifacts. A parallel development direction with a strong mechatronic focus will be the improvement of auxiliary systems such as faster and more flexible robotic sample manipulation devices and novel in situ measurement cells. It is important to emphasize that even with the micro-CT hardware and software available commercially right now, there are vast unexplored fields of applications that are readily accessible by custom-built in situ cells. We believe that photovoltaics, high entropy materials, foodstuff analysis, heterogeneous catalysis, additive manufacturing, and fibrous composite research will be among the first areas where exciting new micro-CT–based developments will appear in the near future.

Declaration of competing interest

The authors declare that they have no known competing financial interests or personal relationships that could have appeared to influence the work reported in this paper.

Acknowledgment

This authors acknowledge the financial support by the Hungarian National Research, Development and Innovation Office through the GINOP-2.3.3-15-2016-00010 and K126065 projects.

References

[1] A.J. Sederman, Magnetic resonance imaging, in: Ind. Tomogr, Elsevier, 2015, pp. 109–133, https://doi.org/10.1016/B978-1-78242-118-4.00004-6.
[2] S. Zaefferer, S.I. Wright, D. Raabe, Three-dimensional orientation microscopy in a focused ion beam–scanning electron microscope: a new dimension of microstructure characterization, Metall. Mater. Trans. 39 (2008) 374–389, https://doi.org/10.1007/s11661-007-9418-9.
[3] T. Hashimoto, G.E. Thompson, X. Zhou, P.J. Withers, 3D imaging by serial block face scanning electron microscopy for materials science using ultramicrotomy, Ultramicroscopy 163 (2016) 6–18, https://doi.org/10.1016/j.ultramic.2016.01.005.
[4] P. Ercius, O. Alaidi, M.J. Rames, G. Ren, Electron tomography: a three-dimensional analytic tool for hard and soft materials research, Adv. Mater. 27 (2015) 5638–5663, https://doi.org/10.1002/adma.201501015.
[5] M. Sun, D. Hu, W. Zhou, Y. Liu, Y. Qu, L. Ma, 3D photoacoustic tomography system based on full-view illumination and ultrasound detection, Appl. Sci. 9 (2019) 1904, https://doi.org/10.3390/app9091904.
[6] J. Deng, Y.H. Lo, M. Gallagher-Jones, S. Chen, A. Pryor, Q. Jin, Y.P. Hong, Y.S.G. Nashed, S. Vogt, J. Miao, C. Jacobsen, Correlative 3D x-ray fluorescence and ptychographic tomography of frozen-hydrated green algae, Sci. Adv. 4 (2018) 1–11, https://doi.org/10.1126/sciadv.aau4548.
[7] C.T. Badea, S.M. Johnston, Y. Qi, K. Ghaghada, G.A. Johnson, Dual-energy micro-CT imaging for differentiation of iodine- and gold-based nanoparticles, in: Med. Imaging 2011 Phys. Med. Imaging, 2011, p. 79611X, https://doi.org/10.1117/12.878043.
[8] S.C. Mayo, A.W. Stevenson, S.W. Wilkins, In-line phase-contrast X-ray imaging and tomography for materials science, Materials (Basel) 5 (2012) 937–965, https://doi.org/10.3390/ma5050937.
[9] J. Oddershede, Sø Schmidt, H.F. Poulsen, H.O. Srensen, J. Wright, W. Reimers, Determining grain resolved stresses in polycrystalline materials using three-dimensional X-ray diffraction, J. Appl. Crystallogr. 43 (2010) 539–549, https://doi.org/10.1107/S0021889810012963.
[10] P.R. Miller, S.C. Mayo, T. Gureyev, S.W. Wilkins, J. Sheffield-Parker, An SEM-based X-ray microtomography system, Microsc. Microanal. (2006) 1592–1593, https://doi.org/10.1017/S1431927606067420.
[11] E.H. Lehmann, A. Kaestner, C. Grünzweig, D. Mannes, P. Vontobel, S. Peetermans, Materials research and non-destructive testing using neutron tomography methods, Int. J. Mater. Res. 105 (2014) 664–670, https://doi.org/10.3139/146.111053.
[12] P. Vontobel, E.H. Lehmann, R. Hassanein, G. Frei, Neutron tomography: method and applications, Phys. B Condens. Matter 385–386 (2006) 475–480, https://doi.org/10.1016/j.physb.2006.05.252.
[13] G.N. Hounsfield, Computerized transverse axial scanning (tomography): Part I. Description of system, Br. J. Radiol. 46 (1973) 1016–1022, https://doi.org/10.1016/0360-3016(94)E0127-6.
[14] J.C. Elliott, S.D. Dover, X-ray microtomography, J. Microsc. 126 (1982) 211–213, https://doi.org/10.1111/j.1365-2818.1982.tb00376.x.
[15] B. Niemann, D. Rudolph, G. Schmahl, X-ray microscopy with synchrotron radiation, Appl. Optic. 15 (1976) 1883, https://doi.org/10.1364/AO.15.001883.
[16] A. Sasov, X-ray nanotomography, Dev. X-Ray Tomogr. IV (2004) 201–211, https://doi.org/10.1117/12.559009.
[17] W. Chao, J. Kim, S. Rekawa, P. Fischer, E.H. Anderson, Demonstration of 12 nm resolution fresnel zone plate lens based soft X-ray microscopy, Optic Express 17 (2009) 17669–17677, https://doi.org/10.1364/oe.17.017669.
[18] A. Sakdinawat, D. Attwood, Nanoscale X-ray imaging, Nat. Photon. 4 (2010) 840–848, https://doi.org/10.1038/nphoton.2010.267.
[19] S.R. Stock, X-ray microtomography of materials, Int. Mater. Rev. 44 (1999) 141–164, https://doi.org/10.1179/095066099101528261.
[20] A. du Plessis, W.P. Boshoff, A review of X-ray computed tomography of concrete and asphalt construction materials, Construct. Build. Mater. 199 (2019) 637–651, https://doi.org/10.1016/j.conbuildmat.2018.12.049.
[21] Y. Arai, A. Yamada, T. Ninomiya, T. Kato, Y. Masuda, Micro-computed tomography newly developed for in vivo small animal imaging, Oral Radiol. 21 (2005) 14–18, https://doi.org/10.1007/s11282-005-0024-5.
[22] A. Kohlbrenner, S. Hämmerle, A. Laib, P. Rüegsegger, A 3D microtomographic system with stacked fan-beam geometry, Nucl. Instruments Methods Phys. Res. Sect. A Accel. Spectrometers, Detect. Assoc. Equip. 443 (2000) 531–539, https://doi.org/10.1016/S0168-9002(99)01045-1.
[23] R.T. Lopes, H.S. Rocha, E.F.O. De Jesus, R.C. Barroso, L.F. De Oliveira, M.J. Anjos, D. Braz, S. Moreira, X-ray transmission microtomography using synchrotron radiation, Nucl. Instruments Methods Phys. Res. Sect. A Accel. Spectrometers, Detect. Assoc. Equip. 505 (2003) 604–607, https://doi.org/10.1016/S0168-9002(03)01157-4.
[24] Y.I. Nesterets, T.E. Gureyev, M.R. Dimmock, Optimisation of a propagation-based x-ray phase-contrast micro-CT system, J. Phys. D Appl. Phys. 51 (2018) 115402, https://doi.org/10.1088/1361-6463/aaacee.
[25] L.A. Feldkamp, L.C. Davis, J.W. Kress, Practical cone-beam algorithm, J. Opt. Soc. Am. A. 1 (1984) 612–619, https://doi.org/10.1364/JOSAA.1.000612.
[26] A. du Plessis, C. Broeckhoven, A. Guelpa, S.G. le Roux, Laboratory x-ray micro-computed tomography: a user guideline for biological samples, GigaScience 6 (2017) 1–11, https://doi.org/10.1093/gigascience/gix027.
[27] J.E. Elkhoury, R. Shankar, T.S. Ramakrishnan, Resolution and limitations of X-Ray Micro-CT with applications to sandstones and limestones, Transp. Porous Media 129 (2019) 413–425, https://doi.org/10.1007/s11242-019-01275-1.
[28] S.R. Stock, MicroCT in practice, in: S.R. Stock (Ed.), Microcomput. Tomogr. Appl., CRC Press, 2009, pp. 85–114, https://doi.org/10.1201/9780429186745.
[29] L. Salvo, M. Suéry, A. Marmottant, N. Limodin, D. Bernard, 3D imaging in material science: application of X-ray tomography, Compt. Rendus Phys. 11 (2010) 641–649, https://doi.org/10.1016/j.crhy.2010.12.003.
[30] T. De Schryver, M. Dierick, M. Heyndrickx, J. Van Stappen, M.A. Boone, L. Van Hoorebeke, M.N. Boone, Motion compensated micro-CT reconstruction for in-situ analysis of dynamic processes, Sci. Rep. 8 (2018) 7655, https://doi.org/10.1038/s41598-018-25916-5.
[31] E. Maire, P.J. Withers, Quantitative X-ray tomography, Int. Mater. Rev. 59 (2014) 1–43, https://doi.org/10.1179/1743280413Y.0000000023.
[32] D.J. Cohen, A. Cheng, K. Sahingur, R.M. Clohessy, L.B. Hopkins, B.D. Boyan, Z. Schwartz, Performance of laser sintered Ti–6Al–4V implants with bone-inspired porosity and micro/nanoscale surface roughness in the rabbit femur, Biomed. Mater. 12 (2017), 025021, https://doi.org/10.1088/1748-605X/aa6810.
[33] D. Nakashima, K. Ishii, M. Matsumoto, M. Nakamura, T. Nagura, A study on the use of the Osstell apparatus to evaluate pedicle screw stability: an in-vitro study using micro-CT, PLoS One 13 (2018), e0199362, https://doi.org/10.1371/journal.pone.0199362.
[34] H.S. Tuan, D.W. Hutmacher, Application of micro CT and computation modeling in bone tissue engineering, Comput. Des. 37 (2005) 1151–1161, https://doi.org/10.1016/j.cad.2005.02.006.
[35] G. Falvo D'Urso Labate, G. Catapano, C. Vitale-Brovarone, F. Baino, Quantifying the micro-architectural similarity of bioceramic scaffolds to bone, Ceram. Int. 43 (2017) 9443–9450, https://doi.org/10.1016/j.ceramint.2017.04.121.

[36] I.F. Cengiz, J.M. Oliveira, R.L. Reis, Micro-CT – a digital 3D microstructural voyage into scaffolds: a systematic review of the reported methods and results, Biomater. Res. 22 (2018) 26, https://doi.org/10.1186/s40824-018-0136-8.
[37] B. Çakmak, E. Ermek, M. Jamil, Micro-computed tomography (micro-CT) in medicine and engineering, in: Micro-Computed Tomogr. Med. Eng., 2020, pp. 171–181, https://doi.org/10.1007/978-3-030-16641-0.
[38] S.M. Chen, H.L. Gao, Y.B. Zhu, H. Bin Yao, L.B. Mao, Q.Y. Song, J. Xia, Z. Pan, Z. He, H.A. Wu, S.H. Yu, Biomimetic twisted plywood structural materials, Natl. Sci. Rev. 5 (2018) 703–714, https://doi.org/10.1093/nsr/nwy080.
[39] A. du Plessis, C. Broeckhoven, Looking deep into nature: a review of micro-computed tomography in biomimicry, Acta Biomater. 85 (2019) 27–40, https://doi.org/10.1016/j.actbio.2018.12.014.
[40] J.E. Rubio, U.K. Chakravarty, An investigation of the aerodynamic performance of a biomimetic insect-sized wing for micro air vehicles, in: Adv. Aerosp. Technol, vol. 1, American Society of Mechanical Engineers, 2016, pp. 1–7, https://doi.org/10.1115/IMECE2016-65303.
[41] R. Niiyama, Micro CT study of soft/elastic structures of beetle toward insect-inspired robotics, in: Proc. 2016 IEEE/SICE Int. Symp. Syst. Integr., 2016, pp. 610–615, https://doi.org/10.1109/SII.2016.7844066.
[42] A. du Plessis, C. Broeckhoven, I. Yadroitsev, I. Yadroitsava, S.G. le Roux, Analyzing nature's protective design: the glyptodont body armor, J. Mech. Behav. Biomed. Mater. 82 (2018) 218–223, https://doi.org/10.1016/j.jmbbm.2018.03.037.
[43] L.A. Burns, Tree joints: biomimetic insights for aerospace composite joints, in: 27th Congr. Int. Counc. Aeronaut. Sci. 2010 vol. 2010, ICAS, 2010, pp. 1979–1988.
[44] M.B. Frank, S.E. Naleway, T.S. Wirth, J.-Y. Jung, C.L. Cheung, F.B. Loera, S. Medina, K.N. Sato, J.R.A. Taylor, J. McKittrick, A protocol for bioinspired design: a ground sampler based on sea urchin jaws, JoVE 2016 (2016) 1–8, https://doi.org/10.3791/53554.
[45] C. Liu, S. Chen, C. Sheng, P. Ding, Z. Qian, L. Ren, The art of a hydraulic joint in a spider's leg: modelling, computational fluid dynamics (CFD) simulation, and bio-inspired design, J. Comp. Physiol. A Neuroethol. Sensory Neural Behav. Physiol. 205 (2019) 491–504, https://doi.org/10.1007/s00359-019-01336-2.
[46] Y. Zhang, A. Reid, J.F.C. Windmill, Insect-inspired acoustic micro-sensors, Curr. Opin. Insect Sci. 30 (2018) 33–38, https://doi.org/10.1016/j.cois.2018.09.002.
[47] B. Wang, B. Pan, G. Lubineau, Morphological evolution and internal strain mapping of pomelo peel using X-ray computed tomography and digital volume correlation, Mater. Des. 137 (2018) 305–315, https://doi.org/10.1016/j.matdes.2017.10.038.
[48] P. Chowdhury, H. Sehitoglu, R. Rateick, Damage tolerance of carbon-carbon composites in aerospace application, Carbon N. Y. 126 (2018) 382–393, https://doi.org/10.1016/j.carbon.2017.10.019.
[49] A. du Plessis, I. Yadroitsava, S.G. le Roux, I. Yadroitsev, J. Fieres, C. Reinhart, P. Rossouw, Prediction of mechanical performance of Ti6Al4V cast alloy based on microCT-based load simulation, J. Alloys Compd. 724 (2017) 267–274, https://doi.org/10.1016/j.jallcom.2017.06.320.
[50] R. Liu, E. Sancaktar, Identification of crack progression in filled rubber by micro X-ray CT-scan, Int. J. Fatig. 111 (2018) 144–150, https://doi.org/10.1016/j.ijfatigue.2018.01.033.
[51] H. Gong, V.K. Nadimpalli, K. Rafi, T. Starr, B. Stucker, Micro-CT evaluation of defects in Ti-6Al-4V parts fabricated by metal additive manufacturing, Technologies 7 (2019) 44, https://doi.org/10.3390/technologies7020044.
[52] Y.C. Wu, C.N. Kuo, M.Y. Shie, Y.L. Su, L.J. Wei, S.Y. Chen, J.C. Huang, Structural design and mechanical response of gradient porous Ti-6Al-4V fabricated by electron beam additive manufacturing, Mater. Des. 158 (2018) 256–265, https://doi.org/10.1016/j.matdes.2018.08.027.
[53] A. Du Plessis, I. Yadroitsev, I. Yadroitsava, S.G. Le Roux, X-ray microcomputed tomography in additive manufacturing: a review of the current technology and applications, 3D print, Addit. Manuf. 5 (2018) 227–247, https://doi.org/10.1089/3dp.2018.0060.
[54] S. Chung, J. Kim, D. Stephan, T. Han, Overview of the use of micro-computed tomography (micro-CT) to investigate the relation between the material characteristics and properties of cement-based materials, Construct. Build. Mater. 229 (2019) 116843, https://doi.org/10.1016/j.conbuildmat.2019.116843.
[55] Í.B. da Silva, X-ray Computed Microtomography technique applied for cementitious materials: a review, Micron 107 (2018) 1–8, https://doi.org/10.1016/j.micron.2018.01.006.
[56] S. Brisard, M. Serdar, P.J.M. Monteiro, Multiscale X-ray tomography of cementitious materials : a review, Cement Concr. Res. 128 (2020) 105824, https://doi.org/10.1016/j.cemconres.2019.105824.
[57] H.K. Bas, W. Jin, N. Gupta, R.K. Behera, In-situ micro-CT characterization of mechanical properties and failure mechanism of cementitious syntactic foams, Cement Concr. Compos. 90 (2018) 50–60, https://doi.org/10.1016/j.cemconcomp.2018.03.007.
[58] I. Netinger Grubeša, B. Marković, M. Vračević, M. Tunkiewicz, I. Szenti, Á. Kukovecz, Pore structure as a response to the freeze/thaw resistance of mortars, Materials (Basel) 12 (2019) 3196, https://doi.org/10.3390/ma12193196.
[59] B. Dong, G. Fang, Y. Liu, P. Dong, J. Zhang, F. Xing, S. Hong, Monitoring reinforcement corrosion and corrosion-induced cracking by X-ray microcomputed tomography method, Cem, Concr. Res. 100 (2017) 311–321, https://doi.org/10.1016/j.cemconres.2017.07.009.
[60] J. Yuan, Y. Liu, Z. Tan, B. Zhang, Investigating the failure process of concrete under the coupled actions between sulfate attack and drying–wetting cycles by using X-ray CT, Construct. Build. Mater. 108 (2016) 129–138, https://doi.org/10.1016/j.conbuildmat.2016.01.040.
[61] P.E. Øren, L.C. Ruspini, M. Saadatfar, R.M. Sok, M. Knackstedt, A. Herring, In-situ pore-scale imaging and image-based modelling of capillary trapping for geological storage of CO_2, Int. J. Greenh. Gas Control. 87 (2019) 34–43, https://doi.org/10.1016/j.ijggc.2019.04.017.
[62] Q. Cao, Y. Gong, T. Fan, J. Wu, Pore-scale simulations of gas storage in tight sandstone reservoirs for a sequence of increasing injection pressure based on micro-CT, J. Nat. Gas Sci. Eng. 64 (2019) 15–27, https://doi.org/10.1016/j.jngse.2019.01.015.
[63] W.G.P. Kumari, P.G. Ranjith, M.S.A. Perera, X. Li, L.H. Li, B.K. Chen, B.L.A. Isaka, V.R.S. De Silva, Hydraulic fracturing under high temperature and pressure conditions with micro CT applications: geothermal energy from hot dry rocks, Fuel 230 (2018) 138–154, https://doi.org/10.1016/j.fuel.2018.05.040.
[64] M.J. Sabti, A.H. Alizadeh, M. Piri, In-situ investigation of the impact of spreading on matrix-fracture interactions during three-phase flow in fractured porous media, Adv. Water Resour. 131 (2019) 103344, https://doi.org/10.1016/j.advwatres.2019.05.017.
[65] Y.A. Alzahid, P. Mostaghimi, N.J. Alqahtani, C. Sun, X. Lu, R.T. Armstrong, Oil mobilization and solubilization in porous media by in situ emulsification, J. Colloid Interface Sci. 554 (2019) 554–564, https://doi.org/10.1016/j.jcis.2019.07.009.
[66] J. Li, Y. Gao, H. Jiang, Y. Liu, H. Dong, Pore-Scale imaging of the oil cluster dynamic during drainage and imbibition using in situ x-ray micro-tomography, Geofluids (2018) (2018) 7679607, https://doi.org/10.1155/2018/7679607.
[67] D.P. Finegan, E. Tudisco, M. Scheel, J.B. Robinson, O.O. Taiwo, D.S. Eastwood, P.D. Lee, M. Di Michiel, B. Bay, S.A. Hall, G. Hinds, D.J.L. Brett, P.R. Shearing, Quantifying bulk electrode strain and material displacement within lithium batteries via high-speed operando tomography and digital volume correlation, Adv. Sci. 3 (2016) 1500332, https://doi.org/10.1002/advs.201500332.
[68] T.M.M. Heenan, C. Tan, J. Hack, D.J.L. Brett, P.R. Shearing, Developments in X-ray tomography characterization for electrochemical devices, Mater. Today 31 (2019) 69–85, https://doi.org/10.1016/j.mattod.2019.05.019.
[69] C. Lim, B. Yan, L. Yin, L. Zhu, Geometric characteristics of three dimensional reconstructed anode electrodes of lithium ion batteries, Energies 7 (2014) 2558–2572, https://doi.org/10.3390/en7042558.
[70] T. Yokoshima, D. Mukoyama, F. Maeda, T. Osaka, K. Takazawa, S. Egusa, S. Naoi, S. Ishikura, K. Yamamoto, Direct observation of internal state of thermal runaway in lithium ion battery during nail-penetration test, J. Power Sources 393 (2018) 67–74, https://doi.org/10.1016/j.jpowsour.2018.04.092.
[71] J. Zhu, X. Zhang, E. Sahraei, T. Wierzbicki, Deformation and failure mechanisms of 18650 battery cells under axial compression, J. Power Sources 336 (2016) 332–340, https://doi.org/10.1016/j.jpowsour.2016.10.064.
[72] D.P. Finegan, M. Scheel, J.B. Robinson, B. Tjaden, M. Di Michiel, G. Hinds, D.J.L. Brett, P.R. Shearing, Investigating lithium-ion battery materials during overcharge-induced thermal runaway: an operando and multi-scale X-ray CT study, Phys. Chem. Chem. Phys. 18 (2016) 30912–30919, https://doi.org/10.1039/C6CP04251A.
[73] R. Carter, B. Huhman, C.T. Love, I. V Zenyuk, X-ray computed tomography comparison of individual and parallel assembled commercial lithium iron phosphate batteries at end of life after high rate cycling, J. Power Sources 381 (2018) 46–55, https://doi.org/10.1016/j.jpowsour.2018.01.087.
[74] A. Yermukhambetova, C. Tan, S.R. Daemi, Z. Bakenov, J.A. Darr, D.J.L. Brett, P.R. Shearing, Exploring 3D microstructural evolution in Li-Sulfur battery electrodes using in-situ X-ray tomography, Sci. Rep. 6 (2016) 35291, https://doi.org/10.1038/srep35291.
[75] A. Rawal, P.V.K. Rao, V. Kumar, A. Kukovecz, A critical review on the absorptive glass mat (AGM) separators synergistically designed via fiber and structural parameters, J. Power Sources 430 (2019) 175–192, https://doi.org/10.1016/j.jpowsour.2019.04.108.
[76] S. Shukla, V. Kumar, P.V. Kameswara Rao, S. Sharma, D. Sebők, I. Szenti, A. Rawal, A. Kukovecz, Probing the three-dimensional porous and tortuous nature of absorptive glass mat (AGM) separators, J. Energy Storage 27 (2020) 101003, https://doi.org/10.1016/j.est.2019.101003.
[77] J. Jankovic, S. Zhang, A. Putz, M.S. Saha, D. Susac, Multiscale imaging and transport modeling for fuel cell electrodes, J. Mater. Res. 34 (2019) 579–591, https://doi.org/10.1557/jmr.2018.458.
[78] B. Kim, F. Hillman, M. Ariyoshi, S. Fujikawa, P.J.A. Kenis, Effects of composition of the micro porous layer and the substrate on performance in the electrochemical reduction of CO2 to CO, J. Power Sources 312 (2016) 192–198, https://doi.org/10.1016/j.jpowsour.2016.02.043.
[79] M. Gebhard, M. Paulisch, A. Hilger, D. Franzen, B. Ellendorff, T. Turek, I. Manke, C. Roth, Design of an in-operando cell for X-ray and neutron imaging of oxygen-depolarized cathodes in chlor-alkali electrolysis, Materials (Basel) 12 (2019) 1275, https://doi.org/10.3390/ma12081275.
[80] T. Kotaka, Y. Tabuchi, P.P. Mukherjee, Microstructural analysis of mass transport phenomena in gas diffusion media for high current density operation in PEM fuel cells, J. Power Sources 280 (2015) 231–239, https://doi.org/10.1016/j.jpowsour.2015.01.111.
[81] R.W. Atkinson, Y. Garsany, B.D. Gould, K.E. Swider-Lyons, I.V. Zenyuk, The role of compressive stress on gas diffusion media morphology and fuel cell

performance, ACS Appl. Energy Mater. 1 (2018) 191–201, https://doi.org/10.1021/acsaem.7b00077.
[82] W.K. Epting, S. Litster, Microscale measurements of oxygen concentration across the thickness of diffusion media in operating polymer electrolyte fuel cells, J. Power Sources 306 (2016) 674–684, https://doi.org/10.1016/j.jpowsour.2015.12.016.
[83] A.D. Shum, D.Y. Parkinson, X. Xiao, A.Z. Weber, O.S. Burheim, I.V. Zenyuk, Investigating phase-change-induced flow in gas diffusion layers in fuel cells with X-ray computed tomography, Electrochim. Acta 256 (2017) 279–290, https://doi.org/10.1016/j.electacta.2017.10.012.
[84] S. Kabir, K. Lemire, K. Artyushkova, A. Roy, M. Odgaard, D. Schlueter, A. Oshchepkov, A. Bonnefont, E. Savinova, D.C. Sabarirajan, P. Mandal, E.J. Crumlin, I.V. Zenyuk, P. Atanassov, A. Serov, Platinum group metal-free NiMo hydrogen oxidation catalysts: high performance and durability in alkaline exchange membrane fuel cells, J. Mater. Chem. A. 5 (2017) 24433–24443, https://doi.org/10.1039/C7TA08718G.
[85] S.J. Normile, D.C. Sabarirajan, O. Calzada, V. De Andrade, X. Xiao, P. Mandal, D.Y. Parkinson, A. Serov, P. Atanassov, I.V. Zenyuk, Direct observations of liquid water formation at nano- and micro-scale in platinum group metal-free electrodes by operando X-ray computed tomography, Mater. Today Energy 9 (2018) 187–197, https://doi.org/10.1016/j.mtener.2018.05.011.
[86] K.A. Nagy, I.Y. Tóth, G. Ballai, Á.T. Varga, I. Szenti, D. Sebők, J. Kopniczky, B. Hopp, Á. Kukovecz, Wetting and evaporation on a carbon cloth type gas diffusion layer for passive direct alcohol fuel cells, J. Mol. Liq. 304 (2020) 112698, https://doi.org/10.1016/j.molliq.2020.112698.
[87] K. Yezerska, A. Dushina, F. Liu, M. Rastedt, P. Wagner, A. Dyck, M. Wark, Characterization methodology for anode starvation in HT-PEM fuel cells, Int. J. Hydrogen Energy 44 (2019) 18330–18339, https://doi.org/10.1016/j.ijhydene.2019.05.114.
[88] Q. Meyer, N. Mansor, F. Iacoviello, P.L. Cullen, R. Jervis, D. Finegan, C. Tan, J. Bailey, P.R. Shearing, D.J.L. Brett, Investigation of hot pressed polymer electrolyte fuel cell assemblies via X-ray computed tomography, Electrochim. Acta 242 (2017) 125–136, https://doi.org/10.1016/j.electacta.2017.05.028.
[89] A. Serov, A.D. Shum, X. Xiao, V. De Andrade, K. Artyushkova, I.V. Zenyuk, P. Atanassov, Nano-structured platinum group metal-free catalysts and their integration in fuel cell electrode architectures, Appl. Catal. B Environ. 237 (2018) 1139–1147, https://doi.org/10.1016/j.apcatb.2017.08.067.
[90] Q. Meyer, J. Hack, N. Mansor, F. Iacoviello, J.J. Bailey, P.R. Shearing, D.J.L. Brett, Multi-scale imaging of polymer electrolyte fuel cells using X-ray micro- and nano-computed tomography, transmission electron microscopy and helium-ion microscopy, Fuel Cell. 19 (2019) 35–42, https://doi.org/10.1002/fuce.201800047.
[91] A. Roy, M.R. Talarposhti, S.J. Normile, I.V. Zenyuk, V. De Andrade, K. Artyushkova, A. Serov, P. Atanassov, Nickel–copper supported on a carbon black hydrogen oxidation catalyst integrated into an anion-exchange membrane fuel cell, Sustain. Energy Fuels. 2 (2018) 2268–2275, https://doi.org/10.1039/C8SE00261D.
[92] F.J. Pinar, M. Rastedt, N. Pilinski, P. Wagner, A. Dyck, Demonstrating feasibility of a high temperature polymer electrolyte membrane fuel cell operation with natural gas reformate composition, Int. J. Hydrogen Energy 42 (2017) 13860–13875, https://doi.org/10.1016/j.ijhydene.2017.03.161.
[93] X. Lu, O.O. Taiwo, A. Bertei, T. Li, K. Li, D.J.L. Brett, P.R. Shearing, Multi-length scale tomography for the determination and optimization of the effective microstructural properties in novel hierarchical solid oxide fuel cell anodes, J. Power Sources 367 (2017) 177–186, https://doi.org/10.1016/j.jpowsour.2017.09.017.
[94] M. Santini, S. Marzorati, S. Fest-Santini, S. Trasatti, P. Cristiani, Carbonate scale deactivating the biocathode in a microbial fuel cell, J. Power Sources 356 (2017) 400–407, https://doi.org/10.1016/j.jpowsour.2017.02.088.
[95] A. Jackiewicz, S. Jakubiak, L. Gradoń, Analysis of the behavior of deposits in fibrous filters during non-steady state filtration using X-ray computed tomography, Separ. Purif. Technol. 156 (2015) 12–21, https://doi.org/10.1016/j.seppur.2015.10.004.
[96] P.-C. Gervais, S. Poussier, N. Bardin-Monnier, G. Karcher, D. Thomas, Combination of Single-Photon Emission and X-Ray Computed Tomography to visualize aerosol deposition in pleated filter, Separ. Purif. Technol. 126 (2014) 52–61, https://doi.org/10.1016/j.seppur.2014.02.011.
[97] A. Charvet, S. Rolland Du Roscoat, M. Peralba, J.F. Bloch, Y. Gonthier, Contribution of synchrotron X-ray holotomography to the understanding of liquid distribution in a medium during liquid aerosol filtration, Chem. Eng. Sci. 66 (2011) 624–631, https://doi.org/10.1016/j.ces.2010.11.008.
[98] P. Kumar, S. Mural, S. Jain, G. Madras, S. Bose, Improving antifouling ability by site-specific silver decoration on polyethylene ionomer membranes for water remediation: assessed using 3D micro computed tomography, water flux and antibacterial studies, RSC Adv. 6 (2016) 88057–88065, https://doi.org/10.1039/C6RA18043D.